

CeO₂ and Nb₂O₅ modified Ni-YSZ anode for solid oxide fuel cell

Pankaj Kr. Tiwari¹ · Suddhasatwa Basu¹

Received: 31 August 2016 / Revised: 15 December 2016 / Accepted: 18 December 2016 / Published online: 12 January 2017
© Springer-Verlag Berlin Heidelberg 2017

Abstract Ni sintering at high temperature (~ 800 °C) operation drastically degrades the performance of Ni-yttria-stabilized zirconia (YSZ) anode in solid oxide fuel cell (SOFC). Mixed ionic and electronic conductive oxides such as CeO₂ and Nb₂O₅ enhance the dispersion of Ni, CeO₂ enhances the redox behavior and promotes charge transfer reactions, and Nb₂O₅ increases the triple phase boundary. In the present work, anode-supported SOFC is fabricated and tested in H₂ fuel at 800 °C. YSZ and lanthanum strontium manganite (LSM)-YSZ are used as the electrolyte and composite cathode with NiO-YSZ, CeO₂-NiO-YSZ, and Nb₂O₅-NiO-YSZ as an anode. The peak power density obtained for the cell with 10% CeO₂-30% NiO-YSZ anode at the 5 and 25 h of operation is 330 and 290 mW cm⁻² which is higher than that for 40% NiO-YSZ anode (275 mW cm⁻² at 5 h). The peak power density obtained for the cell with 10% Nb₂O₅-30% NiO-YSZ anode at the 5 and 25 h of operation is 301 and 285 mW cm⁻² which is higher than that for 40% NiO-YSZ anode (275 mW cm⁻² at 5 h). Physical characterization has been carried to study morphology, elemental analysis, particle size, and phase formation of the fabricated anode before and after cell operation to correlate the cell performance.

Keywords Anode-supported solid oxide fuel cell · CeO₂-NiO-YSZ and Nb₂O₅-NiO-YSZ · Cerium zirconate · Niobium zirconate

This paper has been presented at the 15th Asian Conference on Solid State Ionics, November 27–30, 2016, Patna, India

✉ Suddhasatwa Basu
sbasu@iitd.ac.in

¹ Department of Chemical Engineering, Indian Institute of Technology Delhi, New Delhi 110016, India

Introduction

NiO-yttria-stabilized zirconia (YSZ) is the state-of-the-art composite anode material for solid oxide fuel cell (SOFC) because of excellent catalytic property and high electronic conductivity of Ni in presence of H₂ fuel [1]. To ensure sufficient electronic conductivity and adequate percolation, more than 33% Ni volume is required in Ni-YSZ anode matrix. High Ni content often causes coefficient of thermal expansion (CTE) mismatch between the cell components that leads to cracks in the cell [2]. To decrease Ni loading, infiltration of Ni in porous YSZ is investigated where high electronic conductivity has been reported even at 10–12% Ni loading [3–6]. The lower Ni loading helps in reducing the CTE mismatch during redox cycling and the thermal mismatch between the anode and electrolyte. Fabrication of thick anode support by infiltration technique is a time-consuming process, which requires multiple infiltration and calcination cycles and limits the application of this technique. Sintering at elevated temperature leads to agglomeration of Ni particles, which is another major concern in long term SOFC testing in case of infiltrated anode matrix. Studies on modified Ni-YSZ anode where nickel supported on oxides such as TiO₂, CeO₂, and Nb₂O₅ exhibited suppression in the agglomeration of nickel particles [6–8]. In case of anode fabricated by solid-state reaction route, the zirconia reacts with metal oxides during high temperature sintering at 1450 °C and forms stable zirconate solid solution. Formation of zirconium titanate and cerium zirconate prevents nickel coarsening as well as provides stable SOFC performance as reported by Tiwari and Basu [7, 8]. Insertion of Zr⁴⁺ ions into CeO₂ lattice enhances the reducibility, oxygen storage capacity, thermal stability, and electrical conductivity in Ni-CeO₂-YSZ anode. Further, mixed ionic and electronic conductors (MIEC) such as CeO₂ and Nb₂O₅ help in accelerating the anode gas oxidation [9–11]. MIEC oxides provide

better dispersion of Ni particles, inhibit agglomeration, extend triple phase boundary to wide area of anode matrix, and also enhance redox behavior which are the key requirements for a good catalyst towards fuel oxidation reactions. It is reported that CeO₂-Ni-YSZ provided 20% higher power density than Ni-YSZ anode in syngas at 800 °C [11]. DFT modeling of CeO₂-Ni-YSZ in the form of anode-electrolyte interface points out that the reduction of a ceria with subsequent migration of an oxygen from the YSZ bulk to the reduced ceria is energetically feasible and leads to the accumulation of charge on Ni, accounting for the current generation in SOFC [12]. In SOFC testing environment, Nb₂O₅ reduces to NbO₂ and provides enhanced electronic conductivity to the anode [13, 14]. The aim of the present work is to assess the effect of 10 vol% CeO₂ and Nb₂O₅ addition to Ni-YSZ anode separately on the current-voltage (i-V) performance of anode-supported SOFC. The results in current-voltage characteristics are explained based on electrochemical impedance spectroscopy (EIS), scanning electron microscopy (SEM), energy dispersive X-ray analysis (EDX), transmission electron microscopy (TEM), and X-ray diffraction (XRD).

Materials and methods

NiO-YSZ (40:60), CeO₂-NiO-YSZ (10:30:60), and Nb₂O₅-NiO-YSZ (10:30:60) powders were synthesized by solid-state reaction technique. NiO and/or CeO₂/Nb₂O₅ and YSZ powders in a respective volume ratio were mixed thoroughly for 4 h in a mechanical mortar pestle and sintered at 1450 °C for 5 h in air atmosphere. Thick NiO-YSZ (40:60), CeO₂-NiO-YSZ (10:30:60), Nb₂O₅-NiO-YSZ (10:30:60) anodes, and thin YSZ disks (13 mm, diameter) for button cells were fabricated using die pressing the respective anode along with 20 wt% of starch, pore former, and YSZ (Tosoh, TZ-8Y) powders, as fabricated anode-supported bilayer (anode/electrolyte) pellets were co-sintered in air at 1450 °C. The electrolyte was dense and approximately of 100 μm thick and thickness of porous anode was 300 μm. The composite lanthanum strontium manganite (LSM)-YSZ (70:30) cathode paste was painted on the other side of electrolyte and sintered at 1150 °C in air. Silver wires were attached to the electrodes as current collectors using silver paste. The effective active area of the cell was 0.3 cm². The anode side of the cell was attached to a ceramic tube and sealed using Aremco, Ceramabond. The ceramic tube was connected to a co-axial quartz assembly using Swagelok Ultratorr fitting. The quartz assembly has an inlet tube through which hydrogen was fed to the anode and the outer tube allows unreacted H₂ to exit. The hydrogen flow (40 mL/min) to the system was controlled by a mass flow controller. The cell was heated up to 800 °C in reducing atmosphere at the anode side. The cathode side of the cell was exposed to air. Once the open circuit voltage (OCV) becomes

stable, i-V characteristics and electrochemical impedance spectra of the cell were measured using potentiostat/galvanostat (Versasta 3-400, Ametek). The microstructure, morphology, and elemental analysis of the anode before and after cell operation had been analyzed using scanning electron microscope and energy dispersive spectroscopy (SEM/EDX, Zeiss EVO 50). The particle size and selected area diffraction patterns were observed using HRTEM (TEM, Technai G² 200 kV, FEI). The phase formation and crystallite size of constituent of the anode have been analyzed using XRD (PW 2040/60, X'Pert PRO, Netherlands) with an area detector using a Cu Kα (1.54056 Å) radiation source.

Results and discussion

Ni-YSZ (40:60) anode is tested in anode-supported half-cell Ni-YSZ/YSZ and Ni-YSZ/YSZ/YSZ-LSM full cell at 800 °C in H₂ fuel. The peak power density obtained from bilayer cell is 117 mW cm⁻² at 217 mA cm⁻² current density as shown in Fig. 1a. OCV of 1.03 V indicates that electrolyte is perfectly dense. The ohmic and total polarizations as presented in Fig. 1b are 1.02 and 0.94 Ω cm², respectively. Although not presented here, from SEM, the electrolyte and anode thickness is found to be 100 and 300 μm, respectively. The anode is perfectly adhered to electrolyte even after cell testing and no delamination, cracks, or pin holes in the electrolyte are observed. Ni-YSZ/YSZ/YSZ-LSM button cell provided 275 mW cm⁻² peak power density at 550 mA cm⁻² current density as shown in Fig. 1a. Area specific resistance (ASR) corresponds to the linear portion of the i-V curve of the full cell is ~0.877 Ω cm². The morphology of NiO-YSZ anode before and after cell testing is shown in Fig. 1c, d. NiO and YSZ are uniformly distributed throughout the anode matrix with sufficient porosity as shown in Fig. 1c. The presence of well-connected grains confirms proper sintering of NiO-YSZ anode during fabrication. The average particle size of Ni is ~0.5 μm as presented in Fig. 1c. Some agglomerated particles are also observed in Ni-YSZ anode after cell testing due to the sintering of Ni at 800 °C temperature. It may be concluded from the SEM of anode after cell operation (Fig. 1d) that the backbone structure of the anode is stable and there is no deterioration due to reduction-oxidation during the course of cell operation. HRTEM and selected-area electron diffraction (SAED) patterns of Ni-YSZ (40:60) are presented in Fig. 1e, f. Uniform distribution of Ni particles (15 nm) in anode matrix is shown in Fig. 1e. Diffraction patterns that correspond to Ni is observed from Fig. 1f. Inset of Fig. 1f shows the selected area electron diffraction patterns that correspond to Ni-YSZ (40:60) anode. Although the percentage of NiO loading is slightly higher (40 vol%) than that of the required percolation limit, the button type SOFC gives reasonable performance and it can further be improved by reducing the electrolyte

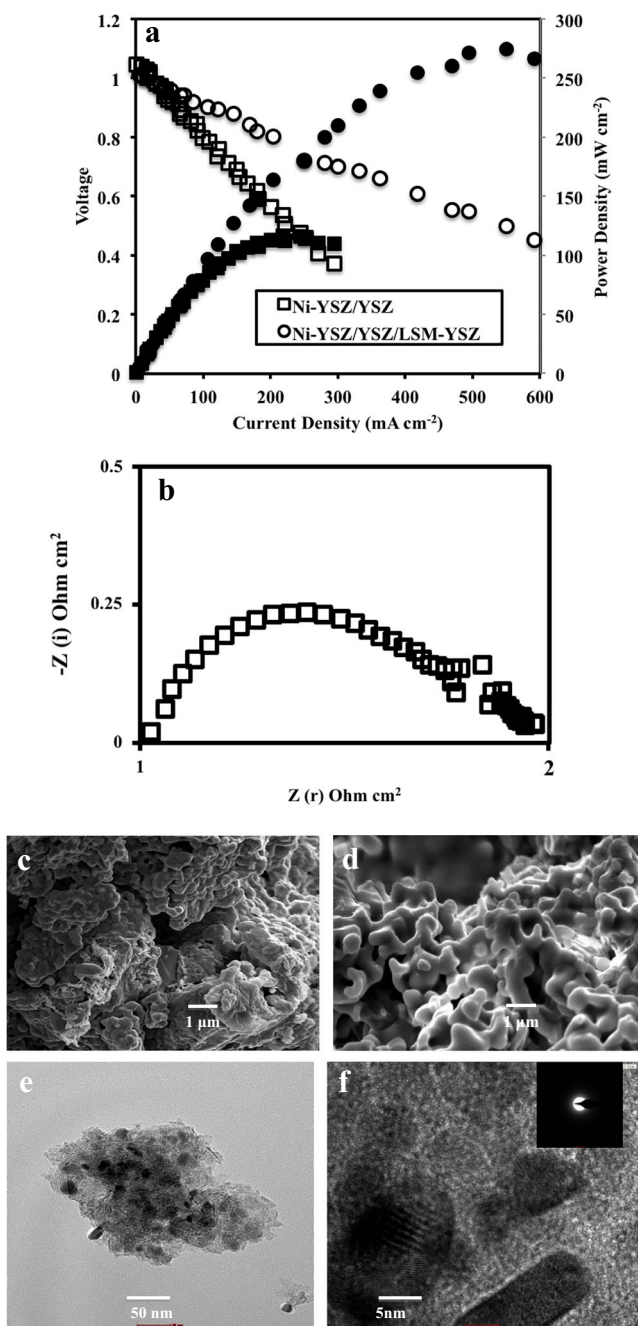


Fig. 1 **a** i-V and i-P characterization of anode-supported half-cell (Ni-YSZ/YSZ) and full cell (Ni-YSZ/YSZ/LSM-YSZ) at 800 °C. **b** Impedance spectra at OCV of half-cell (Ni-YSZ/YSZ) at 800 °C. Ni-YSZ (40:60) anode **c** before and **d** after cell testing. **e**, **f** HRTEM and SAED patterns of Ni-YSZ (40:60) anode

thickness. Effect of 10 vol% CeO₂ or Nb₂O₅ loading on i-V characteristics of Ni-YSZ anode is shown in Figs. 2a and 4a. The quantity of YSZ in anode matrix has been kept constant at 60 vol% as in Ni-YSZ anode matrix but the quantity of Ni is reduced from 40 to 30 vol%, and 10% CeO₂ or Nb₂O₅ is added to the respective anode matrix. The cell with CeO₂-Ni-YSZ (10:30:60) anode provides 332 mW cm⁻²

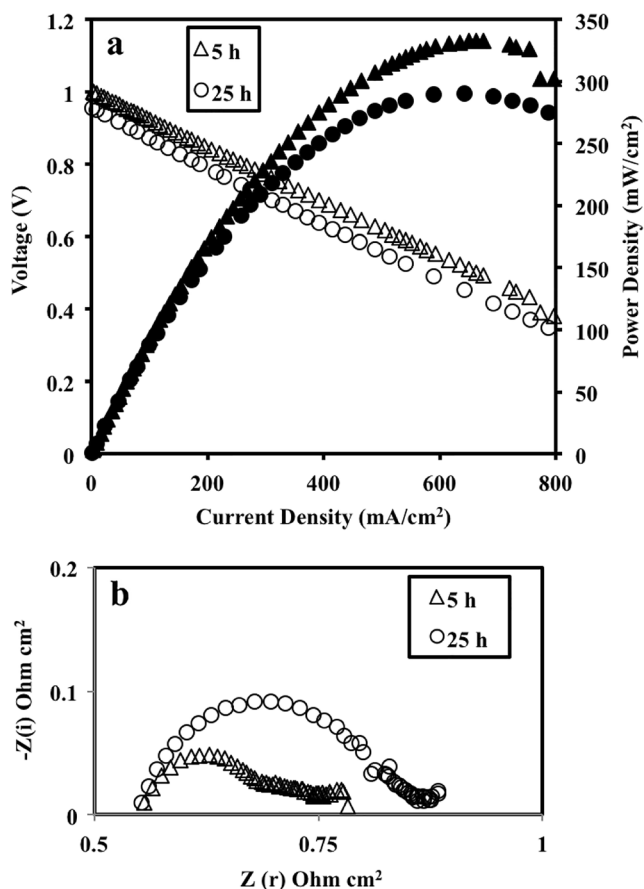
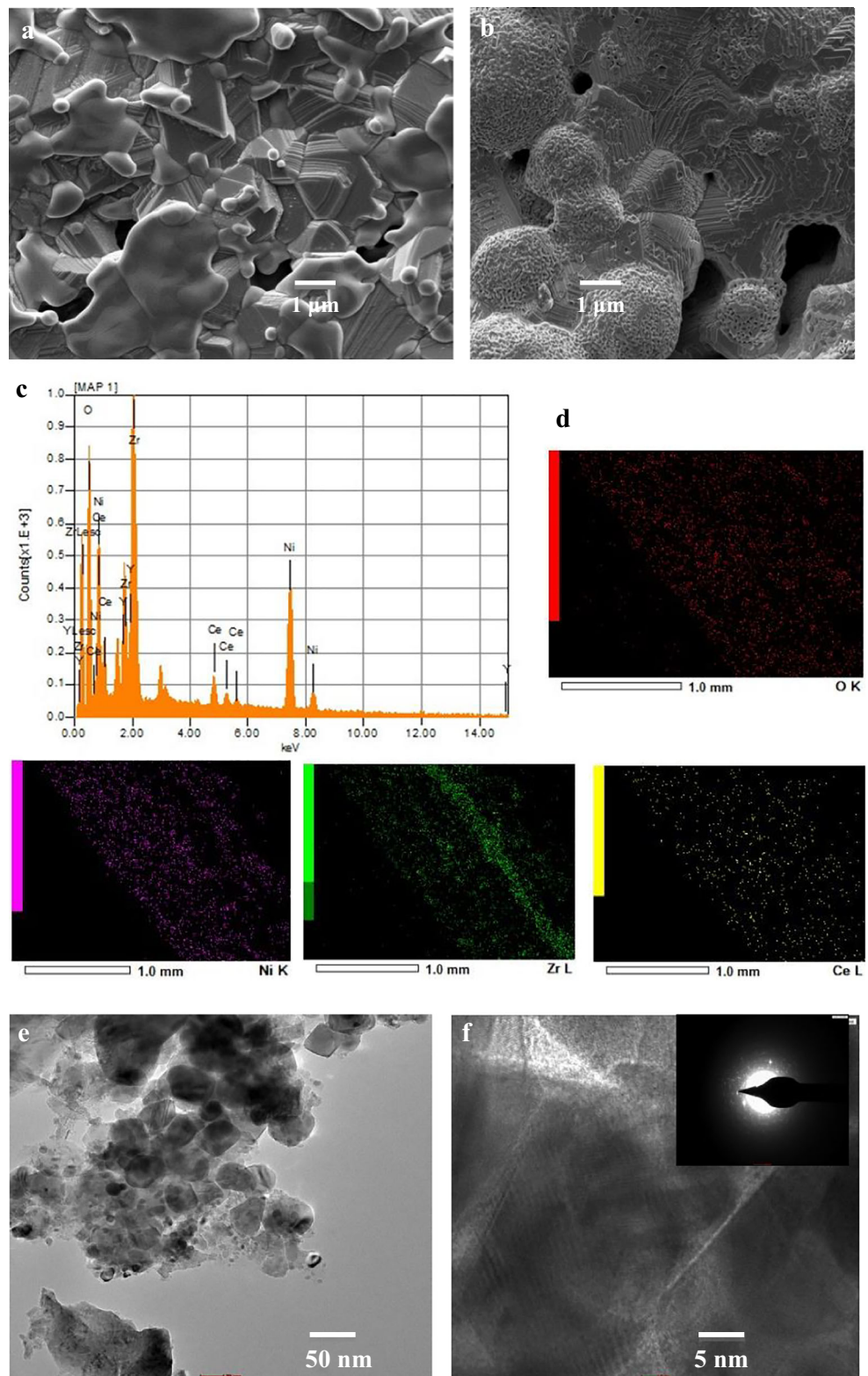


Fig. 2 **a** i-V and i-P characterization of anode-supported cell (CeO₂-Ni-YSZ/YSZ/LSM-YSZ) at 800 °C. **b** Impedance spectra at OCV of anode-supported cell (CeO₂-Ni-YSZ/YSZ/LSM-YSZ) at 800 °C

(675 mA cm⁻²) and 290 mW cm⁻² (642 mA cm⁻²) at 5 and 25 h, respectively. The ohmic resistance is almost constant, ~0.55 Ω cm² till 25 h whereas polarization resistance slightly increases from 0.23 Ω cm² at 5 h to 0.32 Ω cm² at 25 h (Fig. 2b) which corroborates i-V characteristics. It can be inferred that ceria addition not only enhances the performance with respect to Ni-YSZ anode as presented in earlier Fig. 1a but also provides reasonable stability to the cell up to 25 h of operation. Figure 3a, b presents the morphology of anode matrix before and after cell testing with ceria addition. Interconnected grains of 10% CeO₂/Ni-YSZ anode matrix with sufficient porosity can be observed from Fig. 3a. The stair type patterns in anode matrix may be due to the formation of cerium zirconate (CZ) solid solution during sintering at 1450 °C. The formation of cerium zirconate and niobium zirconate is reported earlier by Tiwari and Basu [8]. Well-interconnected Ni particles on CZ surface can be observed from SEM presented in Fig. 3b of anode after cell testing at 25 h. The CZ particles may prevent sintering of Ni particles and helps in sustained performance by providing support to active anode catalyst [8]. Elemental analysis of CeO₂-Ni-YSZ shown in Fig. 3c confirms the presence of constituent

Fig. 3 SEM **a** before cell testing and **b** after cell testing. **c** EDX and **d** elemental mapping after cell testing for 25 h of CeO₂-Ni-YSZ (10:30:60) anode. **e, f** HRTEM and SAED patterns of Ni-CeO₂-YSZ (30:10:60) anode



elements Ce, Ni, O, Y, and Zr in the anode after cell testing. Elemental mapping presented in Fig. 3d confirms the uniform distribution of Ce and Ni throughout the anode matrix.

Uniformly distributed Ni particles on CZ anode matrix can be observed from HRTEM shown in Fig. 3e. Diffraction pattern that corresponds to CeO₂-Ni-YSZ anode is shown in

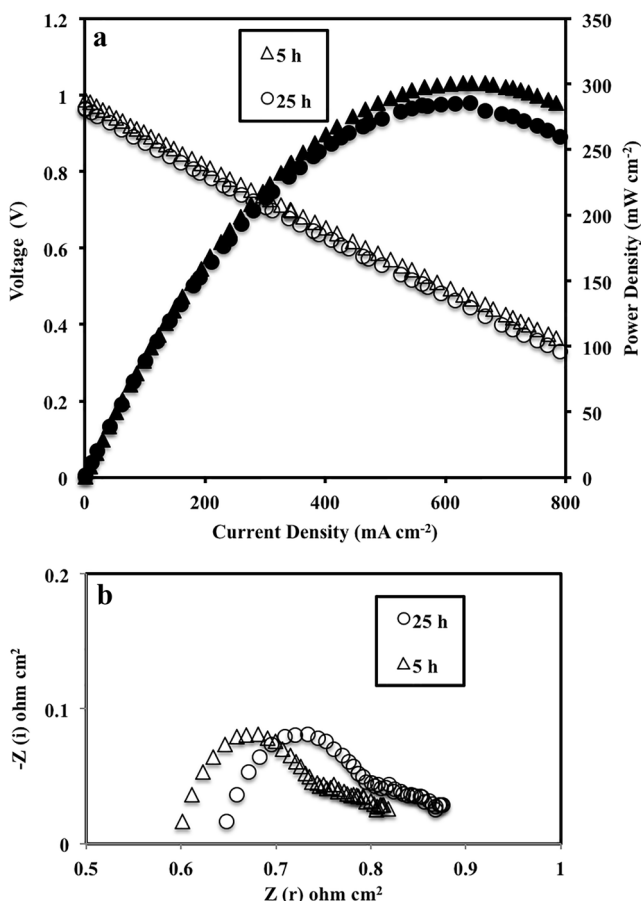
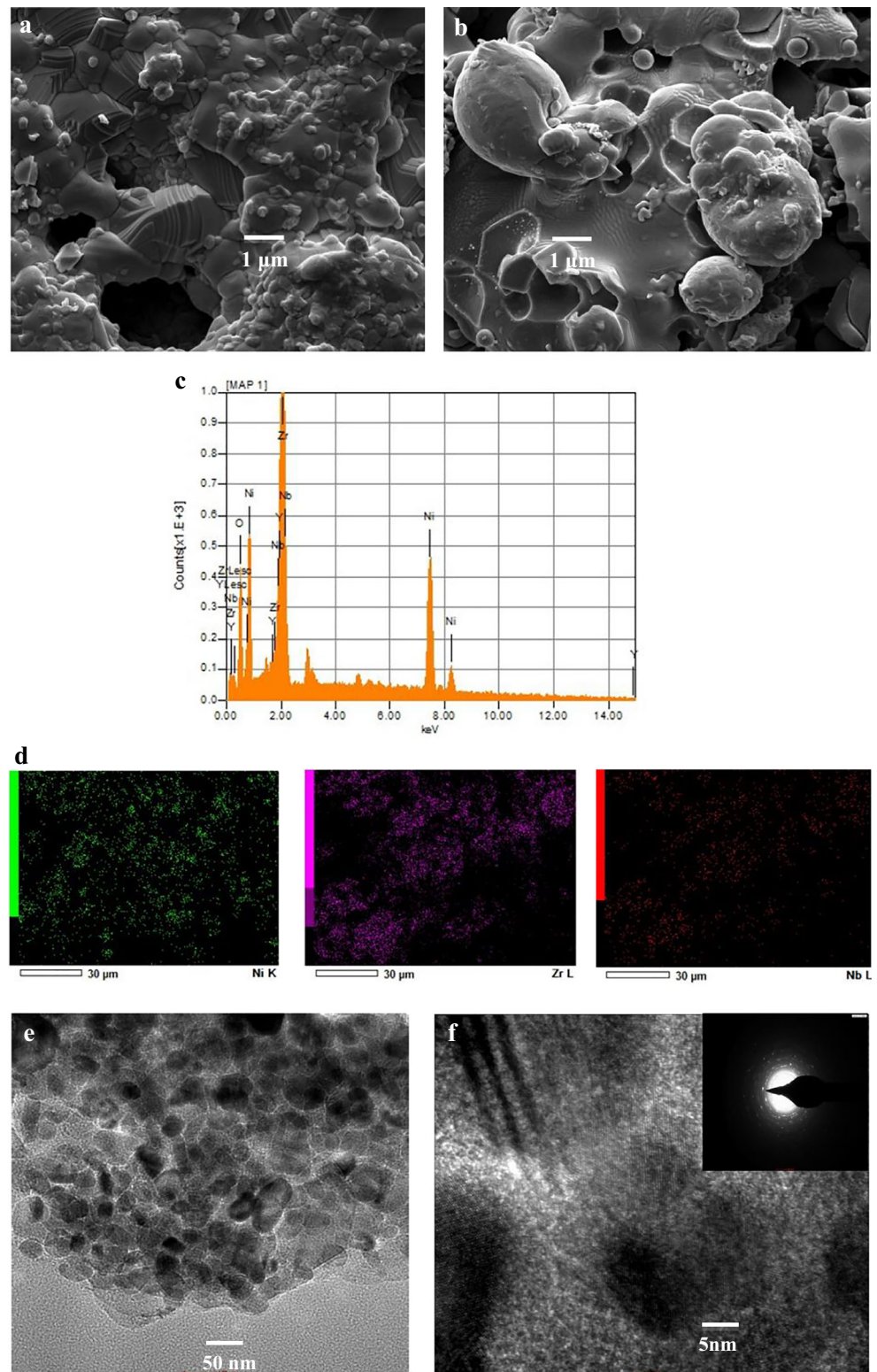


Fig. 4 **a** i-V and i-P characterization of anode-supported cell (Nb₂O₅-Ni-YSZ/YSZ/LSM-YSZ) at 800 °C. **b** Impedance spectra at OCV of anode-supported cell (Nb₂O₅-Ni-YSZ/YSZ/LSM-YSZ) at 800 °C

Fig. 3f. SAED patterns in inset of Fig. 3f show distribution of Ni particles along with the regular crystal patterns. Figure 4a shows the i-V characteristics of SOFC with Nb₂O₅-Ni-YSZ as an anode. The peak power density 301 mW cm⁻² at 630 mA cm⁻² current density is observed at 5 h of operation which decreases to 285 mW cm⁻² at 25 h of cell operation. Nb₂O₅-Ni-YSZ anode shows comparable performance to that of CeO₂-Ni-YSZ which is higher than that of Ni-YSZ anode. The ohmic and polarization resistances of Nb₂O₅-Ni-YSZ (10:30:60) anode-supported cell are 0.6017, 0.6480 and 0.2101, and 0.2138 Ω cm² between 5 and 25 h of operation, as shown in Fig. 4b. The low polarization loss of cell having Nb₂O₅-Ni-YSZ anode is due to reduction of NZ/Nb₂O₅ to NbO₂ in H₂ environment which increases the electronic conductivity of the anode. In case of CeO₂-Ni-YSZ, the ohmic resistance (0.55 Ω cm⁻²) is almost constant until 25 h, which indicates electrolyte performance does not change throughout the cell operation and the catalytic activity as well as the conductivity of CeO₂-Ni-YSZ anode is stable. However, in case of Nb₂O₅-Ni-YSZ anode, ohmic resistance increases from 0.6017 Ω cm⁻² at 5 h to 0.6480 Ω cm⁻² at 25 h, i.e., increment of 0.0463 Ω cm⁻² observed between 5 and 25 h of operation.

The increment in the ohmic resistance may be responsible for the decrease in ionic conductivity of Nb₂O₅-Ni-YSZ. It is known that in reducing atmosphere, Nb₂O₅ get reduced to NbO₂ leading to increase in electronic conductivity and consequently reducing the ionic conductivity. The OCV of the cell that correspond to Ni-YSZ, CeO₂-Ni-YSZ and Nb₂O₅-Ni-YSZ anodes are 1.045, 0.99, and 0.97 V, respectively. The difference in OCV of cell with Ni-YSZ and CeO₂-Ni-YSZ/Nb₂O₅-Ni-YSZ anodes is very small (0.045/0.075 V). The difference in OCV may be due to a sealant problem. Figure 5a, b presents the SEM of 10% Nb₂O₅-Ni-YSZ anode matrix before and after cell testing. Figure 5a shows the well-connected grains of anode backbone of stair type niobium zirconate (NZ) structure. Other than NiO, fine Nb₂O₅ particles can be also observed on NZ surface. Although agglomeration of Ni particles is observed, the anode maintained its backbone structure even after 25 h exposure of H₂ at elevated temperature. EDX shown in Fig. 5c confirms the presence of Nb, O, Y, and Zr elements. Uniform distribution of Ni and Nb in anode is confirmed by the elemental mapping (Fig. 5d). Both the CeO₂-Ni-YSZ (10:30:60) and Nb₂O₅-Ni-YSZ (10:30:60) anodes show excellent thermal and chemical compatibility with other cell components during cell operation as suggested by morphological study. Figure 5e, f presents the HRTEM and SAED patterns of Nb₂O₅-Ni-YSZ (10:30:60) anode matrix. Ni particles are uniformly distributed in support throughout the anode matrix as shown in Fig. 5e. Inset of Fig. 5f shows the regular crystal patterns and distributed Ni in Nb₂O₅-Ni-YSZ anode. Overall XRD of CeO₂-Ni-YSZ (10:30:60) and Nb₂O₅-Ni-YSZ (10:30:60) reveals that the anodes are stable even after 25 h of operation. The result presented shows that 10 vol% addition of ceria or niobia to Ni-YSZ matrix enhances the performance of cell with lower loading of Ni (decreased from 40 to 30 vol%). XRD patterns of NiO-YSZ, CeO₂-NiO-YSZ (10:30:60), and Nb₂O₅-NiO-YSZ (10:30:60) anodes matrices after cell testing are plotted in Fig. 6 to understand phase changes during fabrication as well as due course of accelerated cell testing. CeO₂ and YSZ form solid solutions (cerium zirconate) during high temperature fabrication and remain stable at temperature 800 °C in reducing atmosphere during cell operation [8, 11]. NiO, CeO₂, and cerium zirconate exist as cubic lattice. Niobia reacts with YSZ at high temperature and makes a solid phase (niobium zirconate), which upon reduction forms NbO₂. There is no significant change before and after cell testing in diffraction patterns of CeO₂-NiO-YSZ (10:30:60) and Nb₂O₅-NiO-YSZ (10:30:60) anodes. We have matched XRD data with standard JCPDS files, i.e., #34–0394 for CeO₂ and #30–0873 for Nb₂O₅. A small intensity peak that corresponds to CeO₂ before 30° 2θ angle is observed. It shows that most of CeO₂ had reacted and formed CZ during high temperature sintering. Presence of small intensity peaks that correspond to Nb₂O₅ indicates that some of unreacted Nb₂O₅ are still there other

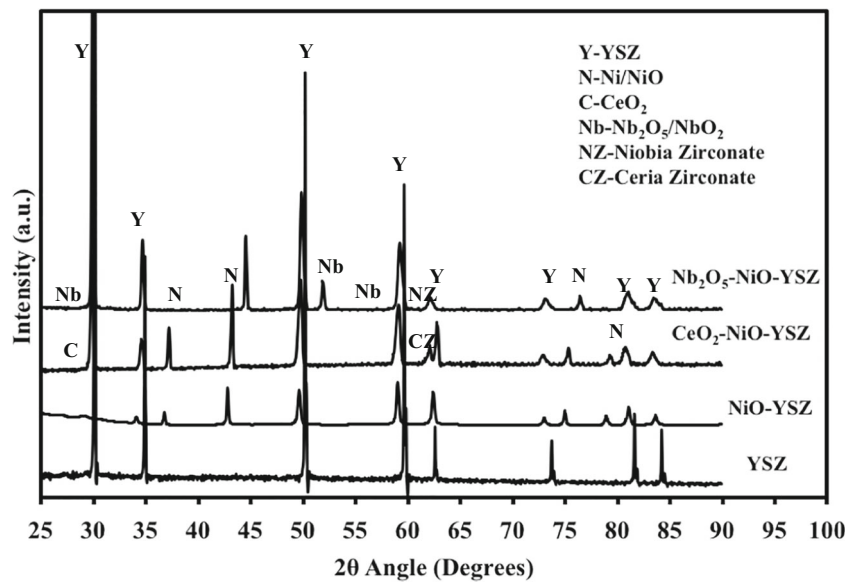
Fig. 5 SEM **a** before cell testing and **b** after cell testing. **c** EDX and **d** elemental mapping after cell testing for 25 h of Nb₂O₅-Ni-YSZ (10:30:60) anode. **e, f** HRTEM and SAED patterns of Ni-Nb₂O₅-YSZ (30:10:60) anode



than NZ phase. No solid reaction between NiO and other constituents of the anode has been observed either during sintering at 1450 °C in air or course of cell operation in reducing atmosphere. Small shifting of YSZ peaks towards lower

angle is observed which is due to the microstructural changes at 1450 °C during sintering of cell. Peaks of CZ and YSZ are overlapping with each other as Zr⁴⁺ ions are getting into the lattice of CeO₂.

Fig. 6 XRD patterns of NiO-YSZ (40:60), CeO₂-Ni-YSZ (10:30:60), and Nb₂O₅-Ni-YSZ (10:30:60) anodes after cell testing



Conclusion

The performance of Ni-CeO₂-YSZ (30:10:60) and Ni-Nb₂O₅-YSZ (30:10:60) anodes is investigated using electrochemical as well as physical characterizations. It is observed that addition of 10 vol% CeO₂ or Nb₂O₅ to 30 vol% Ni-YSZ anode matrix exhibited good catalytic activity during SOFC operation. CeO₂-Ni-YSZ (10:30:60) and Nb₂O₅-Ni-YSZ (10:30:60) anodes are structurally stable even after 25 h of operation. Even though the Ni vol% is reduced to 30 from 40%, the enhanced performance is observed in presence of CeO₂ and Nb₂O₅ because of formation of solid solution, CZ, and NZ, which provided better support in terms of stability and preventing Ni sintering to the anode during cell operation. The as prepared anode-supported button cells with Ni-CeO₂-YSZ and Ni-Nb₂O₅-YSZ anodes showed peak power density 332 and 301 mW cm⁻² in H₂ at 800 °C, respectively.

References

1. Minh NQ (1993) Ceramic fuel cells. *J American Ceramic Soc* 76: 563–588
2. Klemenso T, Mogensen M (2007) Ni-YSZ solid oxide fuel cell anode behavior upon redox cycling based on electrical characterization. *J American Ceramic Soc* 90:3582–3588
3. Singh CA, Krishnan VV (2008) Anode characterization and SOFC performance using Ni-YSZ anodes formed by Ni impregnation methods. *ECS Trans* 6:25–32
4. Klemenso T, Thyden K, Chen M, Wang H-J (2010) Stability of Ni–Yttria stabilized zirconia anodes based on Ni-impregnation. *J Power Sources* 195:7295–7301
5. Singh CA, Bansal L, Tiwari P, Krishnan VV (2009) Strong metal support interaction (SMSI) of infiltrated Ni with TiO₂ in a porous YSZ matrix—a possible method for Ni stabilization. *ECS Transactions* 25(2):1897–1904
6. Tiwari P, Basu S (2013) Ni infiltrated YSZ anode stabilization by inducing strong metal support interaction between nickel and titania in solid oxide fuel cell under accelerated testing. *Int J of Hydrogen Energ* 38(22):9494–9499
7. Tiwari P, Basu S (2014) Performance studies of electrolyte supported solid oxide fuel cell with Ni-YSZ and Ni-TiO₂-YSZ as anode. *J Solid State Electr* 18:805–812
8. Tiwari P, Basu S (2013) Comparison of performance of Ni-CeO₂-YSZ and Ni-Nb₂O₅-YSZ anodes for solid oxide fuel cell. *ECS Trans* 57(1):1545–1552
9. Kanjanaboomalert T, Tzu TH, Sato K (2009) Electrocatalytic activity of an SOFC anode consisting of nickel, cerium oxide, and titanium oxide for the oxidation of methane. *ECS Trans* 16(24):23–29
10. Moon DJ, Park JM, Kang JS, Yoo KS, Hong SI (2006) Cogeneration of a synthesis gas and electricity through internal reforming of methane by carbon dioxide in a solid oxide fuel cell system. *J Ind Engineering Chem* 12(1):149–155
11. Patel S, Jawlik PF, Wang L, Jackson GS, Almansoor A (2012) Impact of cofiring ceria in Ni/YSZ SOFC anodes for operation with syngas and n-butane. *J Fuel Cell Sci Tech* 9:041002-1-7
12. Shishkin M, Ziegler T (2010) The electronic structure and chemical properties of a Ni/CeO₂ anode in a solid oxide fuel cell: a DFT + U study. *J Phys Chem C* 114:21411–21416
13. Reich CM, Kaiser A, Irvine JTS (2001) Niobia based rutile materials as SOFC anodes. *Fuel Cells* 1(3–4):249–255
14. Choi S, Wang J, Cheng Z, Liu M (2008) Surface modification of Ni-YSZ using niobium oxide for sulfur-tolerant anodes in solid oxide fuel cells. *J Electrochemical Soc* 155(5): B449–B454